Research Article

Wiktoria Dubiel, Andrzej Kowalczyk, Aleksandra Jankowska, Marek Michalik, Włodzimierz Mozgawa, Marcin Kobielusz, Wojciech Macyk, and Lucjan Chmielarz*

Silica-titania mesoporous silicas of MCM-41 type as effective catalysts and photocatalysts for selective oxidation of diphenyl sulfide by H_2O_2

https://doi.org/10.1515/gps-2023-0052
received April 21, 2023; accepted August 07, 2023

Abstract: Spherical Ti-MCM-41, synthetized by co-condensation method, presented very promising activity in catalytic and photocatalytic oxidation of diphenyl sulfide with H_2O_2 to obtain diphenyl sulfoxide and diphenyl sulfone. Mesoporous silica materials with various titanium content were analyzed with respect to chemical composition (inductively coupled plasma optical emission spectrometry), structure properties (X-ray diffraction), textural properties (low-temperature N_2 adsorption–desorption), morphology (scanning electron microscopy), forms and aggregation introduced titanium species (diffuse reflectance spectroscopy, Raman spectroscopy), and surface acidity (NH_3-TPD). Titanium introduced in the samples was present mainly in the form of highly dispersed species, presenting catalytic and photocatalytic activities in diphenyl sulfide oxidation with H_2O_2. Efficiency of the reaction increased with an increase in titanium loading in the samples and was significantly intensified under UV irradiation. The role of various Ti species in diphenyl sulfide oxidation was presented and discussed.

Keywords: diphenyl sulfide, oxidation, H_2O_2, Ti-MCM-41

*** Corresponding author: Lucjan Chmielarz,** Department of Chemical Technology, Faculty of Chemistry, Jagiellonian University in Kraków, Gronostajowa 2, 30-387 Kraków, Poland,
e-mail: chmielar@chemia.uj.edu.pl, tel: +48 126862417,
fax: +48 12 686 2750
Wiktoria Dubiel: Department of Chemical Technology, Faculty of Chemistry, Jagiellonian University in Kraków, Gronostajowa 2, 30-387 Kraków, Poland; Doctoral School of Exact and Natural Sciences, Jagiellonian University, Łojasiewicza 11, 30-387 Kraków, Poland
Andrzej Kowalczyk, Aleksandra Jankowska: Department of Chemical Technology, Faculty of Chemistry, Jagiellonian University in Kraków, Gronostajowa 2, 30-387 Kraków, Poland
Marek Michalik: Institute of Geological Sciences, Jagiellonian University in Kraków, Gronostajowa 3a, 30-387 Kraków, Poland
Włodzimierz Mozgawa: Department of Silicate Chemistry and Macromolecular Compounds, Faculty of Materials Science and Ceramics, AGH University of Krakow, Mickiewicza 30, 30-059 Kraków, Poland
Marcin Kobielusz, Wojciech Macyk: Department of Inorganic Chemistry, Faculty of Chemistry, Jagiellonian University in Kraków, Gronostajowa 2, 30-387 Kraków, Poland

1 Introduction

Diphenyl sulfide (Ph_2S) and products of its selective oxidation, such as diphenyl sulfoxide (Ph_2SO) and sulfone (Ph_2SO_2), belong to the group of chemicals important in various industrial branches. Diphenyl sulfide, among others, is used as an intermediate chemical in pesticide, pharmaceutical, and dye industries [1]. Diphenyl sulfoxide is an important chemical used in various organic synthesis as well as a metal extraction agent [2], while diphenyl sulfone is an important reactant in many end-use industry branches, including chemical, pharmaceutical, polymer, agrochemical, as well as paper [3]. The increasing demand for these chemicals is expected in the coming years, mainly in the agrochemical, polymer, pharmaceutical, and paper industries [1–3]. Various oxidants, such as $KMnO_4$, HNO_3, RuO_4, $NaIO_4$, and MnO_2, can be used for selective diphenyl sulfide oxidation [4,5]. Such oxidizing agents have to be used in equimolar amounts of diphenyl sulfide and, in some cases, result in the formation of waste products containing heavy metals [6,7]. The alternative, more environmental-friendly method, is using hydrogen peroxide (H_2O_2) as an oxidation agent for diphenyl sulfide conversion to diphenyl sulfoxide and sulfone. However, in this case, the process has to be conducted under catalytic or photocatalytic regime [7–10]. Titanium oxide in the form of anatase, rutile as well as mixtures of both these forms were reported to be effective photocatalysts of Ph_2S oxidation to Ph_2SO and Ph_2SO_2 using H_2O_2 as oxidant, while for the catalytic reaction without UV irradiation, only anatase and mixture of anatase and rutile were catalytically active, while pure rutile was catalytically inactive [10–12]. Thus, the diphenyl oxidation is possible by classical catalytic process, but UV-assisted reaction (photocatalytic conditions) typically results in a

significant intensification of the product formation [10,11]. Our previous studies [9] have shown that titanosilicate zeolites, such as ferrierite (FER) and its delaminated form (ITQ-6), presented very promising catalytic and photocatalytic activities in Ph_2S oxidation with H_2O_2 resulting in Ph_2SO and Ph_2SO_2. It was shown that conversion of diphenyl sulfide in the presence of microporous three-dimensional FER takes place nearly exclusively on the external surface of the zeolite grain. Penetration of micropores by Ph_2S molecules is limited due to their size, which is estimated to be in the range of 0.24–0.93 nm, depending on the molecules orientation and conformation [9]. While the micropores' diameter in Ti-FER is about 0.55 nm [9]. A significant increase in diphenyl sulfide conversion was found for the delaminated form of FER – ITQ-6. In this case, interlayer space of zeolite is available for the large molecules of Ph_2S. On the other hand, smaller molecules of dimethyl sulfide (DMS) can be effectively oxidized with H_2O_2 to dimethyl sulfoxide and dimethyl sulfone in the presence of both microporous FER and micro-mesoporous ITQ-6 [9]. In this case, the size of DMS molecule is much smaller than size of micropores in FER, and therefore, there are no internal diffusion restrictions. Thus, the accessibility of porous structure, especially by bulky molecules, is a very important point that should be considered in the tailoring of the catalysts. Another important issue is the content of titanium in the samples, which is reported to be catalytically and photocatalytically active in organic sulfates' oxidation with H_2O_2 [7,9]. To overcome the problem of internal diffusion limitations of diphenyl sulfide and products of its oxidation, mesoporous silica materials of MCM-41 type, with various titanium loadings, were tested in the role of the catalysts and photocatalysts of Ph_2S oxidation with H_2O_2. The average pore size in the studied Ti-MCM-41 materials is about 3.2 nm, thus significantly larger than the size of Ph_2S molecules. Mesoporous MCM-41 silica with spherical morphology (shorter channels than in cylindrical MCM-41) was used to limit the distance of reactants' internal diffusion and therefore increase the overall rate of diphenyl sulfide oxidation.

2 Materials and methods

2.1 Catalyst preparation

2.1.1 Synthesis of spherical MCM-41

Spherical MCM-41 material was prepared in accordance with the procedure presented by Liu et al. [13]. Ethanol (POCH) and aqueous ammonia (Sigma Aldrich) hexadecyltrimethylammonium bromide (CTAB; Sigma Aldrich, 98%) were dissolved in distilled water. Then, the mixture was stirred for 15 min, then tetraethyl orthosilicate (TEOS; Sigma Aldrich, 98%) was added and the obtained solution was stirred continuously for the next 2 h. As a result, the synthesis gel with the molar composition ratio of 1 TEOS:0.3 CTAB:11 NH_3:58 ethanol:144 H_2O was obtained. The white solid product was filtrated, washed with distilled water to obtain pH = 7, and then dried at 60°C overnight. Finally, the solid product was calcined at 550°C for 6 h (heating rate of 1°C·min^{-1}). The obtained product is named s-MCM-41.

2.1.2 Synthesis of titanium containing spherical MCM-41

Titanium containing spherical MCM-41 samples were prepared by co-condensation method with the intended Si:Ti molar ratios of 95:5, 90:10, and 80:20. Tetrabutyl orthotitanate (Alfa Aesar, ≥99%) used as a titanium source and TEOS used as a silica source were mixed in the mentioned earlier proportions. The prepared solution was added dropwise to the mixture of water, ethanol, aqueous ammonia, and CTAB and stirred for 2 h. The solid product was recovered by filtration, washed with distilled water to obtain pH = 7, dried at 60°C, and finally calcined at 550°C for 6 h (heating rate 1°C·min^{-1}). As a result, the samples denoted as 3Ti, 8Ti, and 12Ti, respectively, with the Si:Ti intended molar ratios of 95:5, 90:10, and 80:20 were obtained.

2.2 Catalyst characterization

The titanium content in the obtained samples was determined by using inductively coupled plasma optical emission spectrometry (ICP-OES) using an iCAP 7400 instrument (Thermo Science). Analysis was carried out by dissolving solid samples in a mixture of 2 mL of HF (47–51%, Honeywell), 2 mL of HCl (30%, Honeywell), and 6 mL of HNO_3 (67–69%, Honeywell) solutions at 190°C assisted by microwave digestion Ethos Easy system (Milestone).

The X-ray diffractograms were measured with the use of Bruker D2 Phaser. The measurements were performed in the 2 theta ranges of 1–8° and 20–80° with a step of 0.02°. The x-ray diffraction (XRD) patterns were recorded with a counting time of 5 and 1 s per step, respectively.

The morphology of the synthesized materials was examined by scanning electron microscopy (SEM) method. SEM images were recorded using a Hitachi S-4700 microscope (Hitachi Instruments Inc.) equipped with a Noran Vantage analyzer.

The textural parameters of the samples, such as specific surface area and porosity, were determined by N_2 sorption at –196°C using a 3Flex v.1.00 (Micromeritics) automated

gas adsorption system. The samples were outgassed under vacuum at 350°C for 24 h prior to the analysis. The specific surface area of the samples was determined by using BET (Braunauer–Emmett–Teller) equation, while the pore size distributions (PSD) were determined by analysis of the adsorption branch of isotherm by using the Barrett–Joyner–Halenda model. The total pore volume was established by means of the total amount of adsorbed nitrogen at relative pressure p/p_0 = 0.98.

The type of titanium species in the sample structures was analyzed by diffuse reflectance spectroscopy, Raman spectroscopy (UV–Vis DRS). The spectra in the range of 190–900 nm and with a resolution of 2 nm were recorded using Lambda 650 S (Perkin Elmer) spectrophotometer.

Raman spectra of the samples were obtained using a HORIBA Jobin Yvon LabRAM HR micro-Raman spectrometer, equipped with an 789 nm diode Nd:YAG laser, 1800 diffraction grating, as well as 100× Olympus objective. Laser power was adjusted to approximately 9 mW. For each spectrum, four scans were taken and averaged.

The surface acidity of the samples was determined by temperature-programmed desorption of ammonia (NH_3-TPD). The analysis was done in a flow quartz microreactor connected directly to a mass spectrometer with a quadrupole analyzer (PREVAC). Mass flow controllers (Brooks Instrument) were used to adjust the flow rate of the gas mixture supplied to the microreactor. The sample of 50 mg was outgassed in a flow of pure helium (20 mL·min^{-1}) at 550°C for 0.5 h. Subsequently, ammonia sorption was performed in a flow of 1 vol% NH_3/He gas mixture, with a rate of 20 mL·min^{-1} at 70°C for about 90 min. The physisorbed ammonia molecules were removed from the sample surface in a flow of pure helium. Then, desorption of ammonia was monitored with a linear heating rate of 10°C·min^{-1} to 600°C, in a flow of pure helium (20 mL·min^{-1}). Recalculation of the detector signal into the ammonia desorption rate was possible due to the calibration of the QMS with the use of a commercial gas mixture.

2.3 Catalytic and photocatalytic studies

The activity of titanium-containing MCM-41 samples was studied in catalytic and photocatalytic diphenyl sulfide (Ph_2S) oxidation, with hydrogen peroxide as an oxidation agent, to sulfoxide (Ph_2SO) and sulfone (Ph_2SO_2). For the catalytic studies, the reaction mixture was prepared in a round-bottom flask by adding 2 mL of diphenyl sulfide (Sigma Aldrich, 98%) solution (4 mmol·L^{-1}), 20 mL of acetonitrile used as a solvent, 10 µL of bromobenzene (Sigma Aldrich, ≥99.5%) used as an internal standard, as well as 25 mg of the synthesized catalyst. The reaction mixture was stirred (1,000 rpm) at room temperature for 10 min and then 5 µL of 30% hydrogen peroxide (Chempur, pure p.a.) was added. The catalytic tests were conducted with the H_2O_2/sulfide molar ratio of 5. The reaction was conducted in the dark to eliminate the photocatalytic conversion of Ph_2S. The photocatalytic studies were performed with the use of a round quartz cuvette, under UV irradiation, using a xenon lamp (XBO-150, Instytut Fotonowy) as a UV light source. The $CuSO_4$ aqueous solution (10 cm optical path, 0.1 mol·L^{-1}) as NIR and IR filter, as well as a 320 nm cut-off filter, was used to avoid the excitation of Ph_2S and its direct photooxidation. During the irradiation, the suspension was constantly stirred. The reaction progress and selectivity were monitored by high-performance liquid chromatography. The mixture of acetonitrile and water with the relative volume ratio of 70:30 was used as the eluent. The reaction was conducted for 4 h and the reaction mixture samples were taken in regular intervals at 10, 20, 30, 45, and 60 min of the reaction progress and every 30 min afterwards. Prior to the analysis, the liquid samples were filtered (0.22 µm nylon membrane filter) and then analysed using the Flexar chromatograph (PerkinElmer) operating with the analytical C18 column (150 mm × 4.6 mm i.d., 5 µm pore size). The chromatographic analyses were conducted at 25°C and the UV detector was set at 254 nm.

3 Results and discussion

The spherical morphology of pure silica MCM-41 and its modifications with titanium were proved by SEM. As can be seen in Figure 1, all studied samples are composed of spheres of different diameters. In the case of s-MCM-41, most of silica spheres are in the range of 200–700 nm with a small contribution of smaller unregular silica aggregates deposited on silica spheres (Figure 1a). Spheres with similar sizes were identified in the micrograph of MCM-41 modified with the lowest titanium content – 3Ti (Figure 1b). For the 8Ti and 12Ti samples, with higher titanium loadings, apart from spheres, a significant contribution of unshaped aggregates was identified (Figure 1c and d). Moreover, an increase in titanium content in the samples resulted in a tendency to stick to the spheres.

X-ray diffractograms recorded in the low 2 theta range show the presence of three reflections, (100), (110), and (200), which characterize the hexagonal porous structure of MCM-41 (Figure 2). Increasing content of titanium in the samples resulted in decreasing intensity of these reflections, indicating less ordered porous structure. In the case of the sample with the highest titanium loading

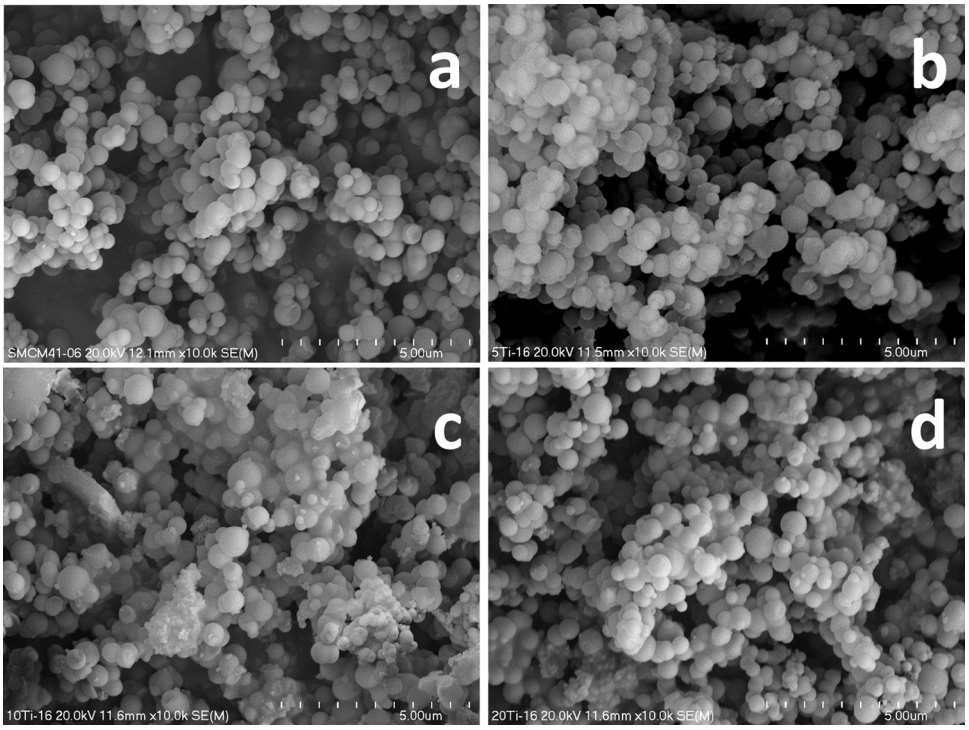

Figure 1: SEM micrographs of S-MCM-41 (a), 3Ti (b), 8Ti (c), and 12Ti (d).

(12Ti), the shift of the (100) diffraction peak into larger 2 theta angle is possibly related to a decrease in the pore size. No reflection characteristics of titanium oxides were found in diffractograms recorded for the studied samples (Figure 2, insert), indicating the deposition of titanium in the form of highly dispersed species. The broad diffraction peak, characteristic of amorphous silica, is centred at about 24° [14].

The nitrogen adsorption–desorption isotherms of pure silica S-MCM-41 and its modifications with titanium are shown in Figure 3, while PSD profiles are presented in Figure 4. Isotherms recorded for the studied samples are classified according to the IUPAC standards as type IV and are typical of mesoporous materials, such as MCM-41 [15,16]. The steep increase in nitrogen uptake at a relative pressure of 0.15–0.30, assigned to the capillary

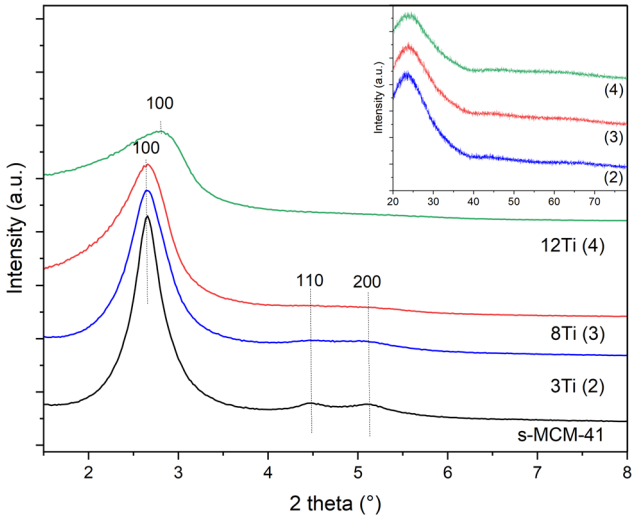

Figure 2: X-ray diffractograms of S-MCM-41, 3Ti, 8Ti, and 12Ti.

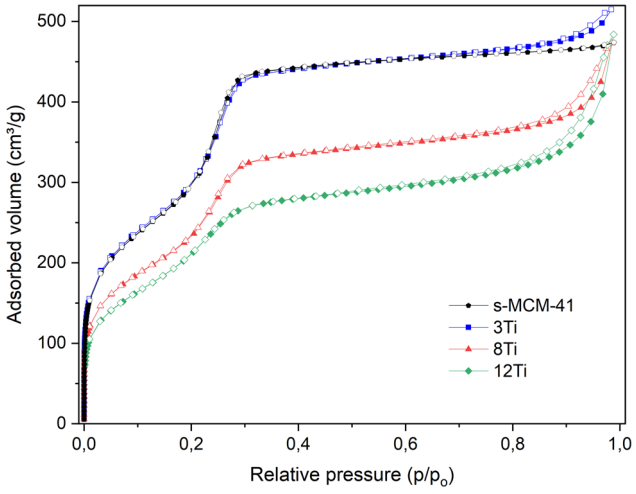

Figure 3: Nitrogen adsorption–desorption isotherms of S-MCM-41, 3Ti, 8Ti, and 12Ti.

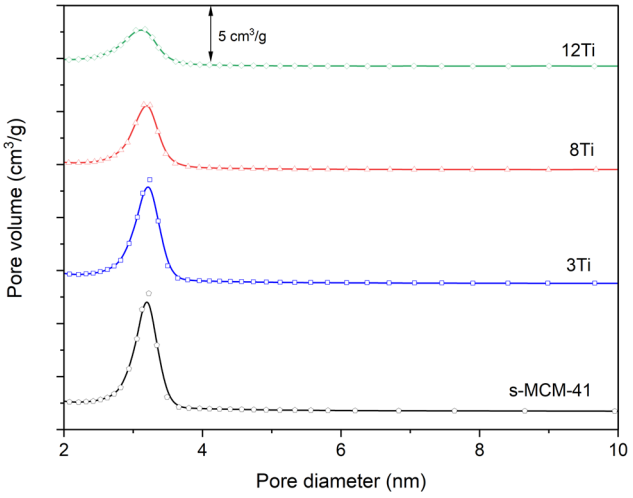

Figure 4: Pore size distribution (PSD) determined for S-MCM-41, 3Ti, 8Ti, and 12Ti.

condensation of nitrogen molecules inside mesopores, is a characteristic feature of these isotherms. Introduction of titanium into silica walls of MCM-41 resulted in a significant decrease in nitrogen uptake, indicating decreased mesopore volume (Figure 3). For the Ti containing MCM-41 samples, an increase in nitrogen adsorption volume above relative pressure of 0.8 is possibly associated with the nitrogen condensation in the space between sticked spheres. This hypothesis is in line with the results of SEM analysis (Figure 1), which showed an increasing tendency to spheres sticking with increasing titanium content in the samples.

The PSD profile of S-MCM-41 proves its uniform distribution of pore sizes with the maximum of the pore diameters (D_p) at about 3.2 nm (Figure 4). In the case of the samples doped with titanium, a decrease in PSD maximum intensity, due to decreased pore volume (V_p), is observed. This effect is less significant for the 3Ti sample with lower titanium content and more significant for the 8Ti sample with higher titanium loading. In the case of the 12Ti sample with the highest titanium loading, the intensity of the PSD profile was significantly reduced, and the maximum of PSD was shifted to about 3.1 nm, indicating a decrease in pore volume and a decrease of their size, which agrees with the results of XRD studies (Figure 2).

In Table 1, the textural parameters of the samples are compared. Specific surface area (S_{BET}) and pore volume (V_p) gradually decreased with an increase in titanium content for the samples containing more than 3 wt% of titanium. The average pore diameter for the S-MCM-41 and its modifications with titanium is about 3.2 nm, however, in the case of the sample with the highest titanium loading (12Ti) decreased to about 3.1 nm.

UV–Vis DRS was used for the analysis of form and aggregation of titanium species in the studied samples (Figure 5). Maxima in the spectra, located in the range of 238–255 nm, are possibly superpositions of three bands related to tetrahedrally coordinated Ti^{4+} cations incorporated into silica matrix, extra framework titanium species – such as octahedrally coordinated Ti^{4+} cations and partially polymerized hexacoordinated Ti species containing Ti–O–Ti bridges. The band assigned to tetrahedrally coordinated Ti^{4+} cations incorporated into silica walls is expected at about 220 nm and corresponds to the ligand-to-metal charge transfer within tetrahedral TiO_4 and O_3TiOH moieties [9,17,18]. Extra-framework titanium species, including isolated Ti^{4+} cations in the octahedral coordination, are represented by band located at about 230–250 nm, while the band at 260–320 nm is characteristic of partially polymerized hexacoordinated Ti species containing Ti–O–Ti bridges [9,19,20]. The shoulder above 320 nm could be assigned to TiO_2 in the form of small anatase and rutile crystallites. The shift of the maxima in the direction of higher values of wavelength with increasing titanium content (Figure 5) indicates the formation of more polymerized titanium species. Similar results were reported by Zakharova et al. [21] for mesoporous silica of SBA-15 type modified with different amounts of titanium. For the

Table 1: Textural parameters, chemical composition, and surface acidity of the sample

Sample	S_{BET} ($m^2 \cdot g^{-1}$)	V_p ($cm^3 \cdot g^{-1}$)	D_p (nm)	Si (wt%)	Ti (wt%)	AS conc. ($\mu mol \cdot g^{-1}$)	AS dens. ($\mu mol \cdot m^{-2}$)	AS conc./Ti ($mol \cdot mol^{-1}$)
S-MCM-41	1,029	0.734	3.2	—	—	—	—	—
3Ti	1,039	0.797	3.2	34.16	3.00	102	0.098	0.16
8Ti	808	0.733	3.2	31.48	7.72	189	0.234	0.12
12Ti	725	0750	3.1	27.87	11.76	260	0.359	0.11

S_{BET} – specific surface area determined by BET method; V_p – pore volume; D_p – average pore diameter; AS conc. – acid sites concentration per 1 g of the sample; AS dens. – acid sites density per 1 m^2 of the sample; AS conc./Ti – ratio of acid sites concentration (determined by NH_3-TPD) and titanium content (determined by ICP-OES).

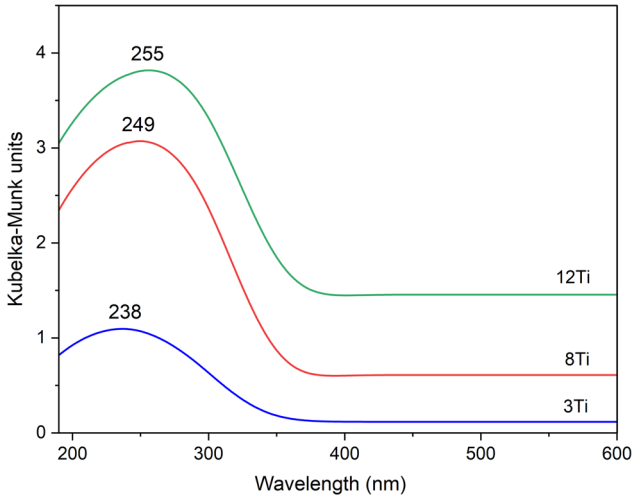

Figure 5: UV–Vis DR spectra recorded for 3Ti, 8Ti, and 12Ti.

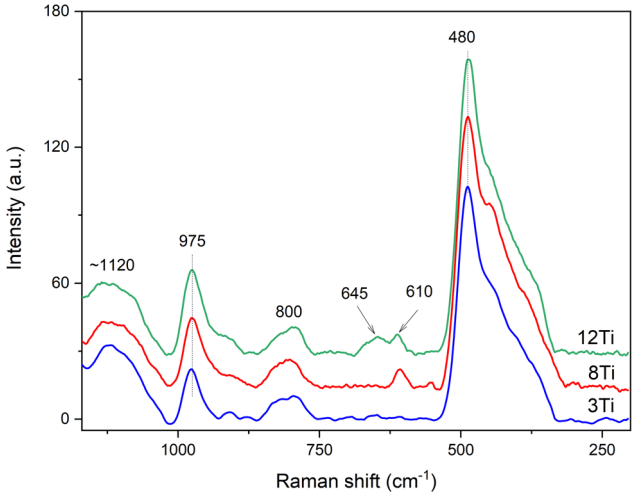

Figure 6: Raman spectra recorded for 3Ti, 8Ti, and 12Ti.

sample with lower titanium loading (7 mol%), the band at about 250 nm was assigned to titanium dispersed on the silica surface framework as tetrahedral Ti^{4+} cations, while the shoulder at about 280 nm to Ti^{4+} cations in the octahedral coordination. These bands are caused by O^{2-} to Ti^{4+} charge transfer in 4- and 6-coordinated titanium cations, respectively [21]. For the SBA-15 samples with higher titanium loadings (12 and 15 mol%), the band at about 315 nm, indicating the presence of ≡Ti–O–Ti≡ bonds, was found. Concluding, UV–Vis DRS analysis of the samples shows that titanium was incorporated into mesoporous silica mainly in the form of highly dispersed species. Moreover, the values of band gaps, determined from UV–Vis DRS measurements for the studied Ti-MCM-41 samples, are in the range of 3.16–3.24 eV (results not shown).

Raman spectra of the studied samples are shown in Figure 6. The bands at about 1120 and 480 cm^{-1} indicate the presence of local Ti–$(O–Si)_4$ units [22,23]. The band at 480 cm^{-1} is related to the bending stretching vibration of the ≡Ti–O–Si≡ species, while the band at about 1120 cm^{-1} to the asymmetric stretching vibration of the ≡Ti–O–Si≡ [24]. The characteristic frequency of ≡Ti–O–Si≡ is sensitive to the coordination environment, and therefore, relatively broad and asymmetric profile of this band may indicate very flexible coordination of titanium incorporated into a silica matrix [25]. The bands at 800 and 975 cm^{-1} are assigned to siloxanol bridge vibrations and Si–O stretching modes of silanol groups, respectively [23,26]. However, the bands at 800 and 975 cm^{-1} can also indicate the presence of titanium in octahedral and tetrahedral coordination, respectively [23,27]. The shoulder on the right side of the band at 480 cm^{-1} is assigned to the presence of extra-framework TiO_2 in the form of small anatase crystallites. Similarly, the small band at about 645 cm^{-1} is observed in the spectrum of the 12Ti sample with the higher titanium loading [22,28]. The small band at about 610 cm^{-1}, identified in spectra of the 8Ti and 12Ti samples, is assigned to small crystallites of rutile [29].

Thus, the analysis of the UV–Vis DR (Figure 5) and Raman (Figure 6) spectra lead to the conclusion that titanium in the samples is present mainly in highly dispersed forms. The low intensive bands, characteristic of rutile, were identified in Raman spectrum of the 8Ti and 12Ti samples. Moreover, small band indicating the presence of anatase was found in a spectrum of 12Ti. These bands were absent in the spectrum of the 3Ti sample. Because the TiO_2 crystallites were not found in the XRD analysis of the studied samples (Figure 2, insert), their size and content are below the detection limit of this method. Thus, it can be concluded that the contribution of small, aggregated titanium species (rutile and anatase) increases with an increase in titanium loading in the Ti-MCM-41 samples.

The method of temperature-programmed desorption of ammonia (NH_3-TPD) was used for the analysis of surface acidity of the samples. The main goal of these studies was the determination of surface exposed Ti species (available for the catalytic operation) contribution. It was assumed that each surface available titanium cation forms one acid site, that can be determined by NH_3-TPD measurement. Ammonia desorption profiles are presented in Figure 7, while acid sites' concentration (AS conc.) and acid sites' density (AS dens.) are compared in Table 1. Any ammonia chemisorption was detected for the pure silica sample – S-MCM-41 (results not shown), while the introduction of titanium into silica samples resulted in the formation of acid sites, identified by ammonia chemisorption (Figure 7). The

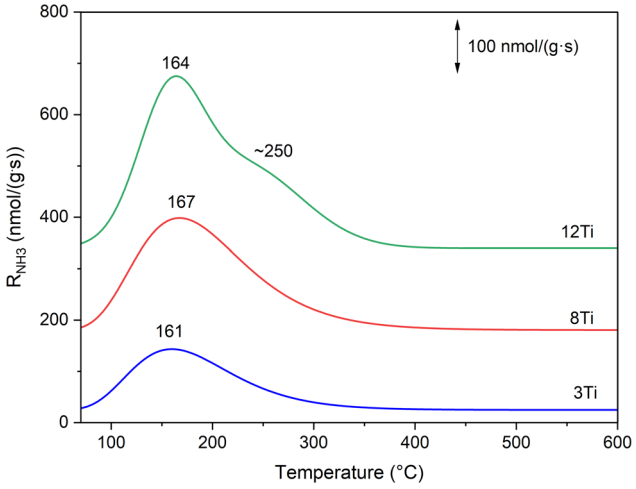

Figure 7: Ammonia desorption profiles measured for 3Ti, 8Ti, and 12Ti.

intensity of ammonia desorption profiles increases with increasing titanium content in the samples. The main desorption peaks, located at about 160–170°C, indicate the presence of relatively weak acid sites, which are possibly associated with the presence of highly dispersed titanium species. In the case of the 12Ti sample with the highest titanium loading, the arm at about 250°C indicates the presence of stronger acid sites, which are possibly associated with more aggregated titanium species. The nature of acid sites in silica-titania systems has been analysed and discussed in the scientific literature [30,31]. Doolin et al. [30] postulated that both Lewis and Brønsted acid sites are formed in such silica-titania samples. The Lewis centres are related to surface unsaturated titanium cations in tetrahedral and octahedral coordination; however, it was also suggested that tetrahedral sites are stronger Lewis acid sites than octahedral sites [30]. On the other hand, Brønsted acid sites can be formed by ≡Si–O–Ti≡ bridge hydrolysis, resulting in the ≡Ti–OH group presenting weak Brønsted-type acidity [30]. Eimer et al. [31] postulated that the presence of Brønsted acid sites in Ti-MCM-41 with high content of titanium is possibly related to the weakening of the ≡SiO–H bond due to the presence of Ti^{4+} ions in the vicinity of the silanol groups. In the case of the larger Ti^{4+} cations' substitution into the positions of the smaller Si^{4+} ions, the bond length of ≡Ti–O–Si≡ is different in comparison to ≡Si–O–Si≡, which results in some structure deformation. Additionally, Ti^{4+} cations in the vicinity of the ≡Si–OH groups may result in changes in the electron density around silicon because of differences in electronegativity as well as the local structure deformations and therefore weakening the ≡SiO–H bonds [31]. Assuming that each surface available titanium cation generates one acid site, the ratio of surface available titanium cations to titanium content in the samples can be estimated (Table 1). This ratio is in the range of 0.11–0.16 and decreases with an increase in titanium content in the samples.

Spherical silica-titania MCM-41 samples were studied in the role of catalysts and photocatalysts of diphenyl sulfide (Ph_2S) oxidation with hydrogen peroxide to diphenyl sulfoxide (Ph_2SO) and diphenyl sulfone (Ph_2SO_2) (Figure 8). Catalytic activity of samples measured in the absence of light increases with an increase in titanium loading. After 4 h of the catalytic test, the Ph_2S conversion (solid lines) reached 70% for 3Ti, 80% for 8Ti, and 96% for 12Ti (Figure 8a). In the case of 3Ti and 8Ti, Ph_2SO was the main reaction product obtained after 4 h of the catalytic test with the selectivity of 67% and 60%, respectively (Figure 8b). The reaction conducted in the presence of 12Ti resulted mainly in Ph_2SO_2, which was obtained with the selectivity of 56% (Figure 8c). Efficiency of Ph_2S oxidation was significantly improved for the process conducted with UV light irradiation. The Ph_2S conversion after 4 h of the catalytic run reached 81% (an increase of 11% in comparison to the reaction conducted in dark) in the case of 3Ti and 99% (an increase of 19%) for 8Ti (Figure 8a, dashed lines). The best photocatalytic and catalytic activities presented the sample with the highest titanium loading, 12Ti, which was able to completely convert Ph_2S during 2.5 h of the catalytic test. Moreover, for the 8Ti and 12Ti samples, a very significant increase in the selectivity to Ph_2SO_2 was observed for the reaction conducted with UV light irradiation (Figure 8c, dashed lines). The selectivity to Ph_2SO_2 reached after 4 h of the catalytic tests 70% and 95% for 8Ti and 12Ti, respectively. Thus, analysis of the results of catalytic and photocatalytic tests shows that oxidation of Ph_2S in the presence of the studied catalysts is possible in the presence and absence of UV irradiation; however, the efficiency of this reaction can be significantly improved by UV irradiation of the reaction mixture. Moreover, the reaction selectivity to deeper oxidized product, Ph_2SO_2, was significantly improved for the UV-assisted reaction. The selectivity to Ph_2SO decreased (Figure 8b), while the selectivity to Ph_2SO_2 increased (Figure 8c), with increasing duration of the catalytic and photocatalytic tests, especially in the case of the 8Ti and 12Ti catalysts, indicating the possible formation of Ph_2SO as a primary product, which in the next step can be oxidized to Ph_2SO_2 ($Ph_2S \rightarrow Ph_2SO \rightarrow Ph_2SO_2$) [10].

Catalytic activity of the samples, both in dark and under UV irradiation, increased with an increase in titanium content in the catalysts; thus, there is no doubt that titanium is responsible for their catalytic and photocatalytic activities in the studied reaction. As it was shown by UV–Vis DRS (Figure 5) and Raman (Figure 6) studies, the catalyst samples contain titanium mainly in the form of highly dispersed Ti species. However, an increase in titanium

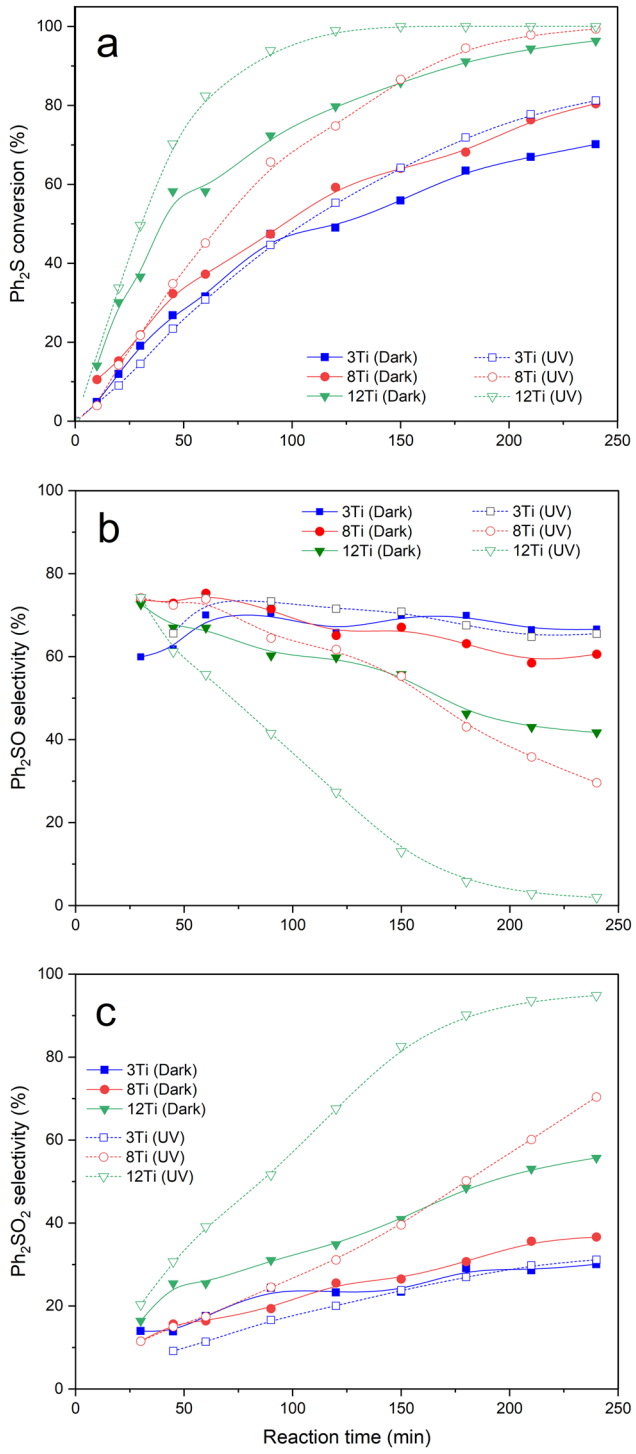

Figure 8: Results of catalytic (dark, solid lines) and photocatalytic (UV, dashed lines) tests for 3Ti, 8Ti, and 12Ti: Ph_2S conversion (a), selectivity to Ph_2SO (b), and selectivity to Ph_2SO_2 (c).

content results in the formation of small rutile and anatase crystallites. Thus, a question arises – which form of titanium species is responsible for catalytic and photocatalytic activation of the MCM-41-based samples. In our previous studies [11], commercial TiO_2 (P25), containing both anatase and rutile, and pure anatase and rutile [10] were tested in the reaction of Ph_2S oxidation with H_2O_2. It was shown that the Ph_2S conversion was observed in dark and was significantly intensified by UV irradiation. Thus, it could be concluded that TiO_2 crystallites are active in both catalytic and photocatalytic Ph_2S oxidation. On the other side, our recent studies of titanosilicate zeolites showed that monomeric titanium cations incorporated into zeolite framework are also active in catalytic and photocatalytic Ph_2S oxidation with H_2O_2 [9]. Thus, both monomeric Ti sites and TiO_2 crystallites have been reported to be active catalysts and photocatalysts of Ph_2S oxidation. Detailed analysis of the results obtained for bulky TiO_2 crystallites [11] and titanosilicate zeolites [9] shows significant differences in selectivity to the reaction products. In the case of P25 selectivity to Ph_2SO_2, the product of deeper Ph_2S oxidation was significantly lower than in the case of titanosilicate zeolites with higher titanium content and opened porous structure. Thus, it could be supposed the higher activity of monomeric titanium cations in zeolite framework than TiO_2 crystallites in Ph_2SO to Ph_2SO_2 oxidation. Of course, this hypothesis needs additional studies to be proved. In the case of the studied samples containing mainly titanium in highly dispersed forms with small contribution of small TiO_2 crystallites, these selectivities to Ph_2SO_2 are higher than for P25 and lower than for titanosilicate zeolites (with higher titanium content and opened porous structure). Thus, the obtained results are in line with the postulated hypothesis. The studies of Ph_2S oxidation with H_2O_2 over pure anatase and pure rutile samples, reported in our previous paper [10], showed that the reaction in the presence of anatase is observed both under catalytic and photocatalytic conditions. In contrast to rutile, which was active only under conditions of photocatalytic oxidation of diphenyl sulfide (no Ph_2S conversion was detected without UV irradiation). Moreover, the reaction conducted in the presence of anatase is more selective to Ph_2SO_2, whereas in the presence of rutile, mainly Ph_2SO was produced. In the case of the studied samples, various titanium species were identified by UV–Vis DRS (Figure 5) and Raman (Figure 6) studies, which contribute to their overall catalytic and photocatalytic properties. The presence of anatase was identified in the case of the 12Ti sample, presenting the highest selectivity to Ph_2SO_2, which supports the hypothesis postulated in our previous paper [10]. The Ph_2S conversion observed for 3Ti and 8Ti at the beginning of the catalytic and photocatalytic tests is very similar (Figure 7). Thus, it seems possible that in the case of highly dispersed Ti species, mainly incorporated into silica walls f, Ph_2S to Ph_2SO oxidation may proceed without UV irradiation. This interesting effect will be analyzed in the future studies.

Catalytic activity of individual titanium sites, expressed as turnover frequency (TOF) values, is presented in Table 2.

Table 2: Turnover frequency (TOF) of Ph_2S to Ph_2SO oxidation determined for 1 h of reaction

Sample	Ti surface sites ($\mu mol \cdot g^{-1}$)	TOF, dark (h^{-1})	TOF, light (h^{-1})	Ref.
3Ti	102*	1,477	1,440	This study
8Ti	189*	938	1,138	This study
12Ti	260*	1,067	1,511	This study
Ti-FER-25	375#	241	532	[9]
Ti-ITQ-6-25	375#	892	1,243	[9]

*Ti surface available sites determined by NH_3-TPD measurements.
#Ti surface available sites determined from chemical analysis (ICP-OES); it was assumed that all Ti sites are available for the catalytic reaction.

TOF values were calculated for the first step of Ph_2S oxidation ($Ph_2S \rightarrow Ph_2SO$). The number of surface Ti sites in the Ti-MCM-41 samples was estimated by NH_3-TPD measurements. The TOF values, determined after 1 h of reaction, are very similar for the sample with the lowest titanium loading, 3Ti, for the reaction conducted under catalytic (dark) and photocatalytic (UV) conditions. For the samples with larger titanium content, 8Ti and 12Ti, frequency of catalytic cycles significantly increased under UV irradiation (Table 2). For comparison, the TOF values for Ph_2S to Ph_2SO oxidation in the presence of Ti zeolitic materials – Ti-FER and Ti-ITQ-6 (in both samples, the Si/Ti molar ratio is about 60) are shown in Table 2. For these zeolitic materials, it was assumed that all Ti sites are located on the surface. The TOF values, determined for Ti-FER under catalytic and photocatalytic conditions, are significantly lower compared to the Ti-MCM-41 catalysts. It could be explained by relatively narrow FER pores, which are unable to accommodate large Ph_2S molecules. Thus, in this case, only Ti sites located on the outer surface of zeolitic grains can effectively participate in catalytic and photocatalytic processes [9]. The TOF values determined for Ti-ITQ-6, characterized by layered structure, are higher than for Ti-FER, but still lower compared to the best catalysts of the Ti-MCM-41 series. In this case, the interlayer space is available for Ph_2S molecules, but small channels in layers are still too small to accommodate large molecules of diphenyl sulfide [9]. Thus, this comparison clearly shows a very important role of porous structure in the conversion of large Ph_2S molecules.

A very important question is related to the role of UV irradiation in the intensification of Ph_2S oxidation with H_2O_2 over highly dispersed Ti species. Some possible mechanisms have been postulated. One of them postulates the formation of titanium-hydroperoxide complexes, ≡Ti–O–O–H, which can decompose hydroxyl radicals, $OH^{\cdot}$, much easier than H_2O_2 [32,33]. Also, small polymeric Ti–O–Ti–O–Ti chains may activate Ph_2S oxidation. In such chains, the reduction of Ti^{4+} to Ti^{3+} by guest species may result in the formation of photocatalytic single-sites active in the formation of $OH^{\cdot}$ radicals from H_2O_2 [34]. It is postulated that such one-dimensional chains can act as an antenna-like system collecting light and forming electron–hole pairs, which similarly to bulky TiO_2, can recombine or diffuse [35]. The role of such dispersed Ti species in the photocatalytic process is still not fully recognized and intensively discussed in the literature [36,37].

4 Conclusions

Spherical Ti-MCM-41 materials, obtained by co-condensation method, presented catalytic, and photocatalytic activities in the reaction of diphenyl sulfide oxidation with H_2O_2 to diphenyl sulfoxide and diphenyl sulfone. Titanium introduced into silica samples was present mainly as highly dispersed species (e.g., monomeric cations, chains), however, for the samples with a larger titanium content also small crystallites of anatase and rutile were identified. Diphenyl sulfide conversion increased with increasing titanium content in the samples. The efficiency of diphenyl sulfide oxidation significantly increased for the reaction conducted under UV irradiation. Also, such photocatalytic conditions significantly intensified the formation of diphenyl sulfone, especially in the case of the sample with the highest titanium content. Results of the catalytic tests indicate Ph_2SO as a primary reaction product, which in the next step can be oxidized to Ph_2SO_2 ($Ph_2S \rightarrow Ph_2SO \rightarrow Ph_2SO_2$).

Acknowledgments: Authors thank the National Science Center (Poland) for funding the project 2018/31/B/ST5/00143.

Funding information: The studies were carried out in the frame of project 2018/31/B/ST5/00143 from the National Science Centre (Poland).

Author contributions: Wiktora Dubiel: synthesis of catalysts, catalytic and photocatalytic studies, XRD, UV–Vis DRS, and NH_3-TPD studies, data analysis, and manuscript

writing; Andrzej Kowalczyk: analysis of textural properties and chemical composition; Aleksandra Jankowska: methodology of catalysts' synthesis; Marek Michalik: SEM measurements; Włodzimierz Mozgawa: Raman spectroscopy measurements; Marcin Kobielusz: methodology of photocatalytic tests and manuscript writing; Wojciech Macyk: methodology of photocatalytic tests and manuscript writing; Lucjan Chmielarz: project administration, data analysis, and manuscript writing.

Conflict of interest: The authors state no conflict of interest.

Data availability statement: The datasets generated during and/or analysed during the current study are available from the corresponding author on reasonable request.

References

[1] Global diphenyl sulfide market 2022 by manufacturers, regions, type and application, forecast to 2028. The Marketsandresearch.biz. Chemical and Material [Internet]. 2022 Mar [cited 2022 December 22]. https://www.marketsandresearch.biz/report/292122/global-diphenyl-sulfide-market-2022-by-manufacturers-regions-type-and-application-forecast-to-2028.

[2] Diphenyl sulfoxide market growth opportunities 2022 to 2028 report contains analysis of recent developments and innovations new product launches upcoming challenges and technology landscape. The MarketWatch. [Internet]. 2022 Oct [cited 2022 December 22]. https://www.marketwatch.com/press-release/diphenyl-sulfoxide-market-growth-opportunities-2022-to-2028-report-containes-analysis-of-recent-developments-and-innovations-new-product-launches-upcoming-challenges-and-technology-landscape-2022-10-05.

[3] Diphenyl Sulfone Market. The Future Market Insights. [Internet]. [cited 2022 December 22]. https://www.futuremarketinsights.com/reports/diphenyl-sulfone-market.

[4] Al-Maksoud W, Daniele S, Sorokin AB. Practical oxidation of sulfides to sulfones by H_2O_2 catalysed by titanium catalyst. Green Chem. 2008;10(4):447–51. doi: 10.1039/B717696A.

[5] Smith MB, March J. March's advanced organic chemistry. 6th edn. New York: Wiley; 2007. p. 1780–3.

[6] Trost BM. The atom economy – A search for synthetic efficiency. Science. 1991;254(5037):1471–7. doi: 10.1126/science.19622.

[7] Přech J, Morris RE, Čejka J. Selective oxidation of bulky organic sulphides over layered titanosilicate catalysts. Catal Sci Technol. 2016;6(8):2775–86. doi: 10.1039/C5CY02083B.

[8] Maurya MR, Chandrakar AK, Chand S. Oxidation of methyl phenyl sulfide, diphenyl sulfide and styrene by oxovanadium(IV) and copper(II) complexes of NS donor ligand encapsulated in zeolite-Y. J Mol Catal A-Chem. 2007;278(1–2):12–21. doi: 10.1016/j.molcata.2007.08.021.

[9] Radko M, Rutkowska M, Kowalczyk A, Mikrut P, Święs A, Díaz U, et al. Catalytic oxidation of organic sulfides by H_2O_2 in the presence of titanosilicate zeolites. Microporous Mesoporous Mater. 2020;302:110219. doi: 10.1016/j.micromeso.2020.110219.

[10] Mikrut P, Święs A, Kobielusz M, Chmielarz L, Macyk W. Selective and efficient catalytic and photocatalytic oxidation of diphenyl sulphide to sulfoxide and sulfone: The role of hydrogen peroxide and TiO_2 polymorph. RSC Adv. 2022;12(3):1862–70. doi: 10.1039/D1RA08364C.

[11] Radko M, Kowalczyk A, Mikrut P, Witkowski S, Mozgawa S, Macyk W, et al. Catalytic and photocatalytic oxidation of diphenyl sulphide to diphenyl sulfoxide over titanium dioxide doped with vanadium, zinc, and tin. RSC Adv. 2020;10(7):4023–31. doi: 10.1039/C9RA09903D.

[12] Radko M, Kowalczyk A, Bidzińska E, Witkowski S, Górecka S, Wierzbicki D, et al. Titanium dioxide doped with vanadium as effective catalyst for selective oxidation of diphenyl sulfide to diphenyl sulfonate. J Therm Anal Calorim. 2018;132:1471–80. doi: 10.1007/s10973-018-7119-9.

[13] Liu S, Lu L, Yang Z, Cool P, Vansant EF. Further investigations on the modified Stöber method for spherical MCM-41. Mater Chem Phys. 2006;97(2–3):203–20. doi: 10.1016/j.matchemphys.2005.09.003.

[14] Maddalena R, Hall C, Hamilton A. Effect of silica particle size on the formation of calcium silicate hydrate [C-S-H] using thermal analysis. Thermochim Acta. 2019;672:142–9. doi: 10.1016/j.tca.2018.09.003.

[15] Leofanti G, Padovan M, Tozzola G, Venturelli B. Surface area and pore texture of catalysts. Catal Today. 1998;41(1–3):207–19. doi: 10.1016/S0920-5861(98)00050-9.

[16] Thommes M, Kaneko K, Neimark AV, Olivier JP, Rodriguez-Reinoso F, Rouquerol J, et al. Physisorption of gases, with special reference to the evaluation of surface area and pore size distribution (IUPAC Technical Report). Pure Appl Chem. 2015;87(9–10):1051–69. doi: 10.1515/pac-2014-1117.

[17] Segura Y, Chmielarz L, Kuśtrowski P, Cool P, Dziembaj R, Vansant EF. Characterisation and reactivity of vanadia–titania supported SBA-15 in the SCR of NO with ammonia. Appl Catal B-Environ. 2005;61(1–2):69–78. doi: 10.1016/j.apcatb.2005.04.011.

[18] Blasco T, Corma A, Navarro MT, Pérez-Parienta J. Synthesis, characterization, and catalytic activity of Ti-MCM-41 structures. J Catal. 1995;156(1):65–74. doi: 10.1006/jcat.1995.1232.

[19] Chmielarz L, Piwowarska Z, Kuśtrowski P, Gil B, Adamski A, Dudek B, et al. Porous clay heterostructures (PCHs) intercalated with silica-titania pillars and modified with transition metals as catalysts for the DeNOx process. Appl Catal B-Environ. 2009;91(1–2):449–59. doi: 10.1016/j.apcatb.2009.06.014.

[20] Corma A, Díaz U, Domine ME, Fornés V. New aluminosilicate and titanosilicate delaminated materials active for acid catalysis, and oxidation reactions using H_2O_2. J Am Chem Soc. 2000;122(12):2804–9. doi: 10.1021/ja9938130.

[21] Zakharova MV, Kleitz F, Fontaine FG. Lewis acidity quantification and catalytic activity of Ti, Zr and Al-supported mesoporous silica. Dalton Trans. 2017;46(12):3864–76. doi: 10.1039/C7DT00035A.

[22] Fan F, Feng Z, Li C. UV Raman spectroscopic studies on active sites and synthesis mechanisms of transition metal-containing microporous and mesoporous materials. Acc Chem Res. 2010;43(3):378–87. doi: 10.1021/ar900210g.

[23] Geidel E, Lechert H, Döbler J, Jobic H, Calzaferri G, Bauer F. Characterization of mesoporous materials by vibrational spectroscopic techniques. Microporous Mesoporous Mater. 2003;65(1):31–42. doi: 10.1016/S1387-1811(03)00505-5.

[24] Li C, Xiong G, Liu JK, Ying PL, Xin Q, Feng ZC. Identifying framework titanium in TS-1 Zeolite by UV resonance Raman spectroscopy. J Phys Chem B. 2001;105(15):2993–7. doi: 10.1021/jp0042359.

[25] Zhang WH, Lu JQ, Han B, Li MJ, Xiu JH, Ying P, et al. Direct synthesis and characterization of titanium-substituted mesoporous molecular sieve SBA-15. Chem Mater. 2002;14(8):3413–21. doi: 10.1021/cm011686c.

[26] Jankowska A, Kowalczyk A, Rutkowska M, Mozgawa W, Gil B, Chmielarz L. Silica and silica–titania intercalated MCM-36 modified with iron as catalysts for selective reduction of nitrogen oxides – the role of associated reactions. Catal Sci Technol. 2020;10(23):7940–54. doi: 10.1039/D0CY01415J.

[27] Hammond C, Tarantino G. Switching off H_2O_2 decomposition during TS-1 catalysed epoxidation via post-synthetic active site modification. Catalysts. 2015;5(4):2309–23. doi: 10.3390/catal5042309.

[28] Li L, Wu P, Yu Q, Wu G, Guan N. Low temperature H_2-SCR over platinum catalysts supported on Ti-containing MCM-41. Appl Catal B-Environ. 2010;94(3–4):254–62. doi: 10.1016/j.apcatb.2009.11.016.

[29] Lubas M, Jasinski JJ, Sitarz M, Kurpaska L, Podsiad P, Jasinski J. Raman spectroscopy of TiO_2 thin films formed by hybrid treatment for biomedical applications. Spectrochim Acta A. 2014;133:867–71. doi: 10.1016/j.saa.2014.05.045.

[30] Doolin PK, Alerasool S, Zalewski DJ, Hoffman JF. Acidity studies of titania-silica mixed oxides. Catal Lett. 1994;25:209–23. doi: 10.1007/BF00816302.

[31] Eimer GA, Casuscelli SG, Chanquia CM, Elías V, Crivello ME, Herrero ER. The influence of Ti-loading on the acid behavior and on the catalytic efficiency of mesoporous Ti-MCM-41 molecular sieves. Catal Today. 2008;133–135:639–46. doi: 10.1016/j.cattod.2007.12.096.

[32] Juan Z, Dishun Z, Liyan Y, Yongbo L. Photocatalytic oxidation dibenzothiophene using TS-1. Chem Eng J. 2010;156(3):528–31. doi: 10.1016/j.cej.2009.04.032.

[33] Lee GD, Jung SK, Jeong YJ, Park JH, Lim KT, Ahn BH, et al. Photocatalytic decomposition of 4-nitrophenol over titanium silicalite (TS-1) catalysts. Appl Catal A-Gen. 2003;239(1–2):197–208. doi: 10.1016/S0926-860X(02)00389-7.

[34] Howe RF, Krisnandi YK. Photoreactivity of ETS-10. Chem Commun. 2001;1(17):11588–9. doi: 10.1039/B104870H.

[35] Usseglio S, Calza P, Damin A, Minero C, Bordiga S, Lamberti C. Tailoring the selectivity of Ti-based photocatalysts (TiO_2 and microporous ETS-10 and ETS-4) by playing with surface morphology and electronic structure. Chem Mater. 2006;18(15):3412–24. doi: 10.1021/cm052841g.

[36] Yan Y, Li C, Wu Y, Gao J, Zhang Q. From isolated Ti-oxo clusters to infinite Ti-oxo chains and sheets: Recent advances in photoactive Ti-based MOFs. J Mater Chem A. 2020;8(31):15245–70. doi: 10.1039/D0TA03749D.

[37] Huang F, Hao H, Sheng W, Dong X, Lang X. Cooperative photocatalysis of dye–Ti-MCM-41 with trimethylamine for selective aerobic oxidation of sulfides illuminated by blue light. J Colloid Interface Sci. 2023;630:921–30. doi: 10.1016/j.jcis.2022.10.052.